Li Li,[1] Shi Bai,[1] and Christian T. Sheline[1,2]

hZnT8 (Slc30a8) Transgenic Mice That Overexpress the R325W Polymorph Have Reduced Islet Zn^{2+} and Proinsulin Levels, Increased Glucose Tolerance After a High-Fat Diet, and Altered Levels of Pancreatic Zinc Binding Proteins

Zinc (Zn^{2+}) is involved in both type 1 diabetes (T1DM) and type 2 diabetes (T2DM). The wild-type (WT) form of the β-cell–specific Zn^{2+} transporter, ZNT8, is linked to T2DM susceptibility. *ZnT8* null mice have a mild phenotype with a slight decrease in glucose tolerance, whereas patients with the *ZnT8 R325W* polymorphism (rs13266634) have decreased proinsulin staining and susceptibility to T2DM. We measured Zn^{2+}, insulin, and proinsulin stainings and performed intraperitoneal glucose tolerance testing in transgenic mice overexpressing *hZnT8 WT* or *hZnT8 R325W* fed a normal or high-fat diet. The *hZnT8 R325W* transgenic line had lower pancreatic [Zn^{2+}]$_i$ and proinsulin and higher insulin and glucose tolerance compared with control littermates after 10 weeks of a high-fat diet in male mice. The converse was true for the *hZnT8 WT* transgenic line, and dietary Zn^{2+} supplementation also induced glucose intolerance. Finally, pancreatic zinc binding proteins were identified by Zn^{2+}-affinity chromatography and proteomics. Increasing pancreatic Zn^{2+} (hZnT8WT) induced nucleoside diphosphate kinase B, and Zn^{2+} reduction (hZnT8RW) induced carboxypeptidase A1. These data suggest that pancreatic Zn^{2+} and proinsulin levels covary but are inversely variant with insulin or glucose tolerance in the HFD model of T2DM suggesting novel therapeutic targets.

Zinc (Zn^{2+}) is involved in the diabetic process, but little is known about its role or the homeostatic mechanisms within the pancreas. In animal models of type 1 diabetes (T1DM), Zn^{2+} chelators, compounds that prevent Zn^{2+} toxicity, knockout of Zn^{2+} transporter 5 (*ZnT5*), and a chronic Zn^{2+}-reduced diet attenuated diabetes incidence and mortality (1–3). However, other studies have suggested that acute Zn^{2+} supplementation could be beneficial (reviewed in Taylor [4]). The wild-type (WT) form of *ZnT8* was linked to susceptibility for type 2 diabetes (T2DM), whereas the *ZnT8 R325W* polymorphism (rs13266634, or RW) decreases susceptibility as demonstrated by genome-wide analyses (5,6). Patients homozygous for the *ZnT8 WT* have increased proinsulin levels (7), which is detrimental for T2DM patients (8). Human ZNT8 (hZNT8) WT is also an important autoantigen in adult-onset T1DM patients who lack other autoantigens, and the R325W polymorphism removes one autoantigenic epitope of hZNT8 (9). Finally, *ZnT8* null mice have a mild phenotype with a slight change in granule morphology and a slight decrease in glucose tolerance (10), suggesting redundancy in the mechanisms for providing Zn^{2+} required for insulin packaging (11).

An animal model of T2DM is the high-fat diet (HFD). Feeding mice a diet from 6 to 16 weeks of age in which 60% of their calories derive from fat induces hyperglycemia, hyperinsulinemia, and glucose intolerance to intraperitoneal

[1]Department of Ophthalmology and the Neuroscience Center of Excellence, Louisiana State University Health Sciences Center, New Orleans, LA

[2]Department of Neurology, Stony Brook University Hospital, Stony Brook, NY

Corresponding author: Christian T. Sheline, christian.sheline@stonybrookmedicine.edu.

glucose tolerance testing (IPGTT) in a manner similar to T2DM patients (12). We propose that Zn^{2+} is transported into the Golgi and endoplasmic reticulum of β-cells for secretory granule incorporation by ZnT5 and ZnT8. Knockout of ZnT5 decreases free secretory Zn^{2+} (3), whereas knockout of ZnT8 decreases both free and some insulin-bound Zn^{2+}, inducing a mild reduction in insulin secretion (10). During chronic inflammation induced by obesity and T2DM, secretory Zn^{2+} homeostasis is disrupted, leading to Zn^{2+}-mediated potentiation of β-cell death or improper processing and packaging of insulin. We generated hZnT8 WT and hZnT8 R325W β-cell–specific transgenic (Tg) mouse lines and characterized them for expression levels, pancreatic $[Zn^{2+}]_i$ and zinc binding proteins (ZBPs), insulin and proinsulin levels, and IPGTT after 10 weeks of an HFD. We tested the hypothesis that excess pancreatic Zn^{2+} induced by overexpression of hZnT8 WT in mice would be detrimental in a model of T2DM, whereas overexpression of hZnT8 R325W in mice would be beneficial.

RESEARCH DESIGN AND METHODS

Generation of hZnT8 Tg Mice and Breeding and Genotyping

Tg rather than knock-in mice were undertaken because overexpression was deemed necessary because of the short duration of the experimental plan. pIns-1 plasmid (13) containing the human insulin promoter (1.9 kB) fused to the rabbit β-globin intron (same construct used in Moynihan et al. [14]) was the expression construct. Human pZnT8WT-EGFP and pZnT8RW-EGFP constructs (15) were used as templates for PCR reactions using the ZnT8 cloning primers (Supplementary Table 1) to introduce appropriate restriction enzyme sites for cloning.

Zn^{2+} Transporter Gene Expression

Total RNA from harvested mouse pancreata was extracted with 0.5 mol/L guanidinium isothiocyanate. For details of the method, see Han et al. (16) and the Supplementary Data online.

Animal Trials and HFD

All studies were conducted according to the Institutional Animal Care and Use Committee (Louisiana State University Health Sciences Center), the Public Health Service Guide for the Care and Use of Laboratory Animals, U.S. Department of Agriculture regulations, and the American Veterinary Medical Foundation Panel on Euthanasia.

At 6 weeks of age, the animals were randomly divided into eight groups containing six mice in each group, such that researchers were blinded to genotype and diet. Groups 1 and 2 were hZnT8 WT-X40 Tg− and Tg+, each fed with normal diet (ND) (2019, Harlan) (3), groups 3 and 4 were hZnT8 WT-X40 Tg− and Tg+ fed with 60% HFD (TD.06414, Harlan) (Supplementary Table 2), and groups 5 and 6 and groups 7 and 8 were the same but with hZnT8 R325W-T12 Tg mice. Additional groups of hZnT8 WT-X28, hZnT8 R325W-T8, and hZnT8 R325W-T16 lines were similarly

performed. At 16 weeks of age, IPGTT was performed, and plasma, serum, and pancreata were collected for further investigation. In addition, C57BL/6J mice were fed with ND, HFD, and HFD Zn^{2+} deficient (HFDD) (60% fat, 1 mg Zn^{2+}/kg diet EWS) (TD.10872, Harlan) (Supplementary Table 2) plus 1, 60, or 260 mg Zn^{2+}/kg diet using ZnSO4 drinking water from 6 to 16 weeks and IPGTT was performed and tissues were collected.

IPGTT and Insulin Measurements

Glucose tolerance was assessed by IPGTT at 16 weeks of age. Mice were fasted for 5–6 h, weighed, and D-glucose (1.5 mg glucose/g body weight) was injected intraperitoneally. Glucose in saphenous vein blood was measured at 0, 15, 30, 45, 60, and 120 min using a blood glucose monitoring system (OneTouch, glucose oxidase). Insulin was measured in duplicate from plasma using enzyme-linked immunosorbent assays (EMD Millipore, Darmstadt, Germany).

Insulin/Proinsulin Immunohistochemistry and Zn^{2+} Staining With Zinpyr-1

Mice were anesthetized, plasma and serum were generated, and they were killed 24 h after IPGTT. Fresh-frozen pancreata were sectioned and sequentially stained for zinc (5 μmol/L zinpyr-1 [ZP1]), anti-insulin, or anti-proinsulin as previously described (3). Islet images were captured at identical exposures using a Nikon TS-100 and SIS software. The adjacent slide was fixed in 2% paraformaldehyde/2% glutaraldehyde and developed using a monoclonal antibody to proinsulin (G3–9A8, DSHB, University of Iowa; 1:200) and goat anti-mouse Cy3. Islet fluorescence intensity was measured by National Institutes of Health software ImageJ from six to eight slides per animal and six animals per group. Identical threshold intensities were calculated and integrated by area and compared between each experimental group.

Zinc-Agarose Chromatography

A 50-mg piece of pancreas from each of three animals fed an HFD of each group (hZnT8WT-X40, hZnT8RW-T12, and C57BL/6J control) were rapidly homogenized into 2 mL of lysis buffer (50 mmol/L Tris [pH 7.5], 125 mmol/L NaCl, 5% glycerol, 0.4% IGEPAL CA-630, 10 μmol/L $MgCl_2$, 1 mmol/L phenylmethylsulfonyl fluoride, and fresh 1× protease inhibitor without EDTA) and cleared. The supernatant was dialyzed in lysis buffer, cleared (Input), and incubated for 2 h with 200 μL of high-affinity Zn^{2+}-agarose beads (Lamda Biotech, St. Louis, MO) at 4°C. The slurry was poured into a mini-column, and the unbound (FT) fraction collected. The column was washed with lysis buffer and eluted (Eluate) with 3 × 400 μL 500 mmol/L imidazole in lysis buffer; the beads were boiled in SDS buffer, each fraction was collected, and aliquots were saved.

Protein Isoelectric Focusing/SDS-PAGE

The input, FT, and eluted proteins from C57BL/6J controls were precipitated, and 50 μg of each fraction labeled with Cy5, Cy3, and Cy2, respectively, for Fig. 5. Eluates from

ZnT8WT and ZnT8RW were labeled with Cy2 and Cy3, and the FT from ZnT8WT was labeled with Cy5 for Fig. 6 (17). Samples were first run on isoelectric-focusing gel strips (pH 3–10 nonlinear, 24 cm; GE Healthcare, Piscataway, NJ), equilibrated, and run in the second dimension on 10% SDS-PAGE gels. These two-dimensional gels were scanned using a Typhoon 9400 Variable Mode Imager and spot detection and quantification were performed using DeCyder differential analysis software DIA, version 5.0 (GE Healthcare). Spots with at least fivefold greater abundance in the elution than the FT and with sufficient Sypro protein staining (~20–50 ng) were excised and trypsin digested using the automated Spot Handling Workstation (GE Healthcare).

Liquid Chromatography–Mass Spectrometry

The trypsin-digested peptides were resuspended in 0.1% formic acid/2% acetonitrile, loaded into a Dionex PepMap C18 trap column, and separated by a New Objective Reversed Phase C18 Picofrit column/emitter (Woburn, NJ). A total of 0.1% formic acid aqueous solution and 0.1% formic acid in acetonitrile were used as buffer A and buffer B, respectively. The gradient elution at 250 nL/min starts at 5%, to 25% buffer B in 20 min, to 60% buffer B in 10 min, to 80% buffer B in 15 min plus 10 min. A blank run was inserted between sample runs to reduce cross-contamination. All spectra were acquired on a Thermo Fisher LTQ-XL linear ion trap mass spectrometer (Waltham, MA) coupling with an Eksigent NanoLC 2D (Dublin, CA).

Statistical Analyses

Values are the mean ± SEM. Differences in RT-PCR, ZnT8 levels, and blood glucose were analyzed by one-way ANOVA between Tg+ and Tg− animals followed by a Bonferroni test, with $P \leq 0.05$ defined as statistically significant.

For determination of significance of the stained pancreatic sections, we used the SAS program to analyze the data by applying the three-way ANOVA test to determine the effect of three nominal predictor variables on a continuous outcome variable. Here the three predictor variables are strain (ZnT8R325W vs. ZnT8WT), treatment (HFD vs. ND), and transgene (Tg+ vs. Tg−). The continuous variable is raw-integrated density of the insulin-, ZP1-, or proinsulin-stained pancreatic sections ($n = 36$), with $P \leq 0.05$ defined as statistically significant.

RESULTS

RT-PCR Was Performed on Each of the hZnT8WT and hZnT8RW Tg Mouse Lines

Nine *hZnT8 WT* and nine *hZnT8 RW* Tg mouse lines were generated, and total pancreatic RNA was isolated from each, reverse transcribed, and 25 cycles of PCR performed to determine relative *ZnT8* RNA expression between lines (top, Supplementary Fig. 1). GAPDH expression was used as an internal control (bottom, Supplementary Fig. 1). Several high- and low-expressing lines were determined.

Mice Expressed the hZnT8 Transgene Predominantly in the Pancreas

ZnT8 WT 549+ (X-40) and *ZnT8 R325W* 8038+ (T-12) were chosen as the high-expressing lines for further study and were backcrossed to C57BL/6J for 10 generations. Pancreas, thymus, brain, and liver from these lines were collected and RNA made. RT-PCR was performed using 25 cycles, and the products run on agarose gels as shown in Supplementary Fig. 2. The expression was highest in pancreas, with thymus and brain expressing much lower levels, and no detectable expression in liver as expected for the insulin promoter (18).

qRT-PCR Was Performed on Lines Chosen for High or Low Expression

Real-time quantitative PCR was performed using *GAPDH* as an internal control, and the quantitation is presented in Supplementary Table 3 for hZnT8, mZIP4, and mZnT8. Lines X-40 and T-12 were chosen for further study of high-expressing lines for *ZnT8 WT* and *ZnT8 RW*, respectively. *ZnT8 RW* lines T-16 and T-8 were chosen for low-expressing lines, and *ZnT8 WT* X-28 line was an intermediate expressor. The expression of mZIP4 was reduced in the X-40 pancreas and increased in the T-12 pancreas, whereas mZnT8 was unaffected (Supplementary Table 3). mZIP4 was studied because it is preferentially expressed in the pancreas and varies inversely with zinc levels (G. Andrews, personal communication), confirming the ZP1 staining results in these Tg lines. Protein levels of hZnT8 could not be determined because the commercially available antibody did not recognize the protein in a Western blot (data not shown). Low levels of an appropriately sized pancreatic protein were present in a high-resolution 5–20% gradient SDS-PAGE gel from Tg+ mice and were not present in Tg− mice (data not shown).

Zn²⁺, Proinsulin, and Insulin Staining Were Determined for Each of the Chosen Lines Fed an HFD or ND

Groups of male mice ($n = 6$ for each Tg line) were exposed to an HFD or ND from 6 to 16 weeks of age. ZP1 staining was performed to determine the levels of pancreatic, stainable Zn^{2+}. Insulin and proinsulin immunohistochemistry were performed on adjacent sections after postfixation. *hZnT8 RW* had significantly decreased Zn^{2+} and proinsulin staining and increased insulin staining compared with Tg− littermates. *hZnT8 WT* had significantly increased Zn^{2+} and proinsulin staining and decreased insulin staining compared with Tg− littermates (Figs. 1 and 2 for HFD and Supplementary Figs. 3 and 4 for ND). The threshold-integrated density of the staining intensity from all of the photomicrographs was determined and is summarized in Table 1. There was a significant difference in Zn^{2+}, insulin, or proinsulin levels in *hZnT8 RW* fed an HFD compared with those fed a ND. In *hZnT8 WT*, there was a significant difference in Zn^{2+} and insulin levels but not in proinsulin levels dependent on dietary fat. There was a significant difference in Zn^{2+}, insulin, and proinsulin levels between *hZnT8 RW* and *hZnT8*
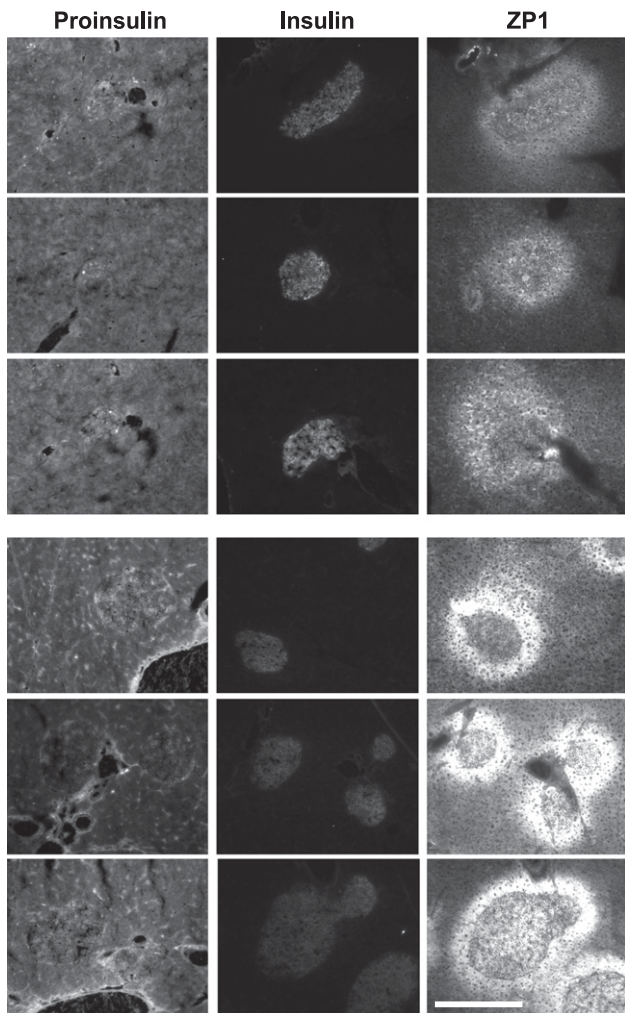
Figure 1—Zn^{2+}, proinsulin, and insulin staining of *hZnT8 RW* male mice (line T-12) after an HFD from 6 to 16 weeks of age. Pancreatic sections (10 μm) from three different 16-week-old HFD-fed *hZnT8* T-12 Tg+ mice (top panels) and three different HFD-fed Tg− mice (bottom panels) were stained with anti-proinsulin (exposure time 100 ms), anti-insulin (exposure time 500 ms), and ZP1 (exposure time 200 ms) at magnification ×100. Scale bar represents 400 μm.

WT Tg+ lines and Tg− littermates fed an HFD. There was a significant difference in Zn^{2+} and insulin but not in proinsulin staining between the RW and WT lines fed a ND.

Glucose Tolerance in Male ZnT8WT, ZnT8RW, and Tg− Littermates After an HFD or ND

IPGTT was performed at 16 weeks of age, and the summarized data are presented in Fig. 3. There was a significant decrease in glucose tolerance for the *ZnT8 WT* line, X-40, in both ND and HFD conditions compared with Tg− littermates. Conversely, there was a significant increase in glucose tolerance for the *ZnT8 RW* line, T-12, only in HFD conditions. Low-expressing *ZnT8 RW* lines had no effect on glucose tolerance. An alternate *ZnT8 WT* line with slightly lower expression levels (X-28) had a less significant decrease in glucose tolerance (data not shown).

Plasma Insulin Levels

Insulin levels were measured (in ng/mL) at 0 min and 30 min (fasting) and 24 h (fed) after IPGTT. ND control mice had 0.19 ± 0.02,* 0.39 ± 0.05,* and 2.1 ± 0.31,* respectively. HFD control mice had 1.1 ± 0.26, 2.58 ± 0.31, and 6.2 ± 0.55, respectively. HFD ZnT8WT mice had 1.02 ± 0.21, 1.7 ± 0.22,* and 5.5 ± 0.5, respectively. HFD ZnT8RW mice had 1.15 ± 0.28, 3.25 ± 0.42,* and 6.75 ± 0.61, respectively. HFDD + 260 ppm zinc had 1.0 ± 0.19, 1.65 ± 0.20,* and 5.45 ± 0.48, respectively. The asterisk indicates a significant difference from insulin levels in HFD control mice at the same time point at $P < 0.05$ ($n = 6$).

Increasing Zn^{2+} Through Diet Decreases Glucose Tolerance

C57BL/6J male mice (same genetic background as ZnT8 Tg− mice) were exposed to an HFD, an HFD reduced

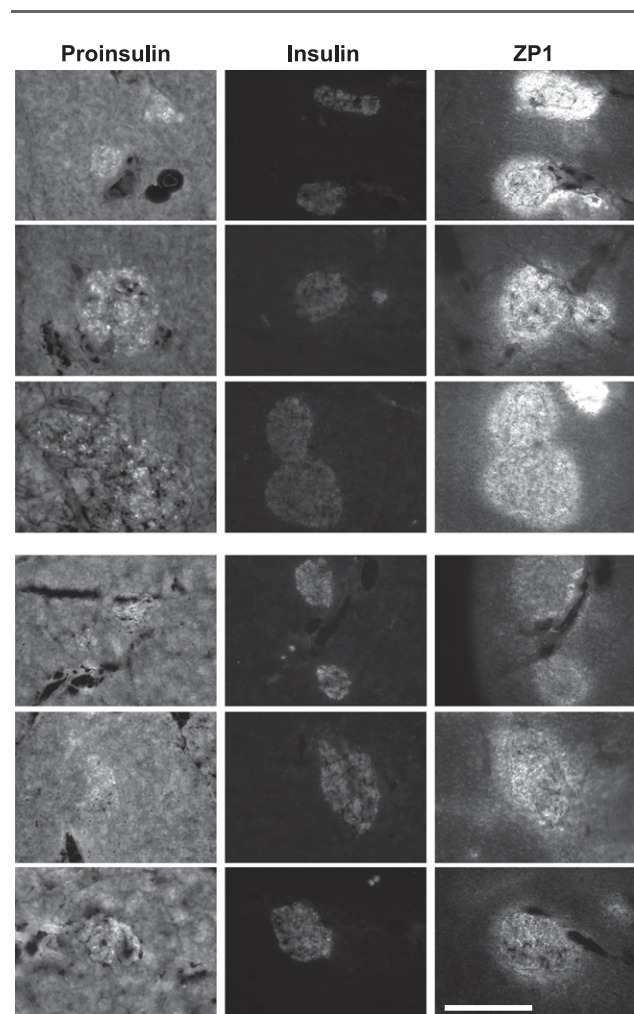**Figure 2**—Zn^{2+}, proinsulin, and insulin staining of *hZnT8 WT* male mice (line X-40) after an HFD from 6 to 16 weeks of age. Pancreatic sections from three different 16-week-old HFD-fed *hZnT8* X-40 Tg+ mice (top panels) and three different HFD-fed Tg− mice (bottom panels) were stained with anti-proinsulin (exposure time 100 ms), anti-insulin (exposure time 500 ms), and ZP1 (exposure time 200 ms) at magnification ×100. Scale bar represents 400 μm.

Table 1—Quantitation of threshold-integrated density of proinsulin, insulin, and Zn^{2+} staining in RW and WT Tg+ and Tg− mice fed an HFD or ND

	ZP1	Insulin	Proinsulin
RW HFD Tg+	458 ± 83[a1,c1,d1]	479 ± 52.6[a2,c2,d2]	199 ± 20[a3,c3]
RW HFD Tg−	782 ± 87	343 ± 30.6	284 ± 78
RW ND Tg+	804 ± 120[b1]	121.4 ± 18[b2]	116 ± 8.9[b3]
RW ND Tg−	620 ± 116	50.9 ± 9.6	240 ± 35
WT HFD Tg+	828 ± 138[e1,f1]	48.1 ± 9.6[e2,f2]	204 ± 21.3[e3]
WT HFD Tg−	466 ± 57	80.5 ± 9.2	137 ± 16.4
WT ND Tg+	301 ± 56	31.2 ± 6.4	205 ± 8.5
WT ND Tg−	646 ± 78	31.2 ± 11	206 ± 33

Values are the average $\times 10^4 \pm$ SEM in relative fluorescence units of threshold-integrated density from 3–4 independent experiments ($n = 15$–25). [a1,a2,a3] indicate a significant difference between ZnT8RW Tg+ and Tg− mice fed an HFD in pancreatic ZP1, insulin, and proinsulin staining, respectively. [b1,b2,b3] indicate a significant difference between ZnT8RW and ZnT8WT Tg+ mice fed a ND in pancreatic ZP1, insulin, and proinsulin staining, respectively. [c1,c2,c3] indicate a significant difference between ZnT8RW Tg+ mice fed an HFD vs. ND in pancreatic ZP1, insulin, and proinsulin staining, respectively. [d1,d2] indicate a significant difference between ZnT8RW and ZnT8WT Tg+ mice fed an HFD in pancreatic ZP1, insulin, and proinsulin staining, respectively. [e1,e2,e3] indicate a significant difference between ZnT8WT Tg+ and Tg− mice fed an HFD in pancreatic ZP1, insulin, and proinsulin staining, respectively. [f1,f2] indicate a significant difference between ZnT8WT Tg+ and Tg− mice fed a ND in pancreatic ZP1 and insulin staining, respectively.

Zn^{2+} (2 mg Zn^{2+}/kg), an HFD normal Zn^{2+} (61 mg Zn^{2+}/kg), and an HFD excess Zn^{2+} (261 mg Zn^{2+}/kg) from 6 to 16 weeks and compared with ND for IPGTT. There was a trend toward an increase in glucose tolerance for the HFD reduced Zn^{2+} compared with the HFD normal Zn^{2+}, with a single time point achieving significance. Conversely, there was a significant decrease in glucose tolerance for the HFD excess Zn^{2+} compared with the HFD normal Zn^{2+} (Fig. 4). This decreased glucose tolerance for the HFD excess Zn^{2+} diet was accompanied by a significant decrease in insulin levels and staining and an increase in zinc staining (3) and proinsulin staining (data not shown and above).

Pancreatic ZBPs Are Secretory, Mitochondrial, and Energy Metabolic Proteins, and Some of Their Levels Are Modulated by Pancreatic Zinc Concentrations

Pancreatic extracts from control mice on HFD were analyzed for ZBPs using zinc-agarose affinity chromatography and proteomics, and proteins were identified (Fig. 5 and Table 2). Only soluble proteins between 10–150 kD with intermediate zinc affinity can be identified using this method. Carboxypeptidase A1 (CpA1) and α-amylase bind Zn^{2+}, showing that the technique is working. Additional identified proteins play roles in mitochondrial and cellular energy metabolism (succinyl-CoA:3-ketoacid-CoA transferase [SCOT], methylmalonate semialdehyde dehydrogenase [MMSDH], nucleoside diphosphate kinase A and B [NDPKA and -B], and α-aminoadipic semialdehyde dehydrogenase). ZBPs from pancreatic extracts of ZnT8WT versus ZnT8RW were analyzed by proteomics. Of these identified pancreatic ZBPs, NDPKB was significantly increased ($>$fivefold) in the pancreas of ZnT8WT (high zinc) Tg mice, as was actin. CpA1 was significantly increased in the pancreas of ZnT8RW (low zinc) Tg mice (Fig. 6).

DISCUSSION

We have generated and characterized Tg mouse lines that overexpress *hZnT8 WT* and *hZnT8 RW* under the control of the insulin promoter for *1*) expression at the RNA level, *2*) expression at the protein level, *3*) organ-specific expression, *4*) stainable Zn^{2+} levels, *5*) insulin and proinsulin levels, *6*) IPGTT after ND or HFD, *7*) the effects of dietary Zn^{2+} on HFD-induced glucose intolerance in C57BL/6J mice, and *8*) ZBPs and their differential expression. Overexpression of the *hZnT8 WT* gene increases pancreatic Zn^{2+} and proinsulin levels and decreases insulin and glucose tolerance. Conversely, overexpression of the *hZnT8 RW* gene decreases pancreatic Zn^{2+} and proinsulin levels and increases insulin and glucose tolerance. Altering dietary Zn^{2+} has similar effects on glucose tolerance after an HFD. We identified pancreatic ZBPs and show that CpA1 is induced by low zinc and NDPKB is induced by increased zinc.

There are two superfamilies of mammalian Zn^{2+} transporters (19,20), and members from each family function in β-cells. Solute carrier 39A (Slc39A) family members, named ZIPs, import Zn^{2+} into cells, and solute carrier 30A (Slc30a) family members, named ZnTs, function in Zn^{2+} efflux and transport into vesicular compartments (20). These transport proteins function as multimers (21). *ZnT3* knockout mice do not load Zn^{2+} in synaptic vesicles and therefore are resistant to neuronal injury after light damage, global ischemia, or hypoglycemia (22,23 and C.T.S. and L. Wei, unpublished data). The lethal milk mouse has a mutation in the *ZnT4* gene causing toxic Zn^{2+}-deficient milk (24). Deletion of *ZnT5* results in poor growth, osteopenia, low body fat, muscle weakness, and male-specific cardiac death (25). ZNT5 functions as a heterodimer putting Zn^{2+} into the general secretory pathway. ZNT8 is β-cell specific, and overexpression of ZNT8 in INS-1E cells increases cellular Zn^{2+} content, increases sensitivity to Zn^{2+} toxicity, and
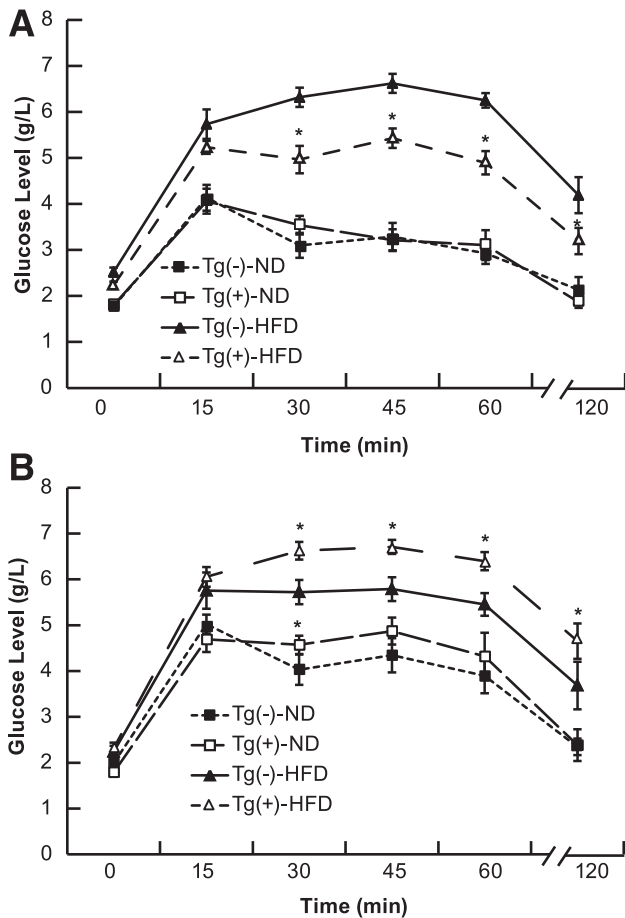
Figure 3—Intraperitoneal glucose tolerance in *ZnT8 RW* T-12 (*A*) and *ZnT8 WT* X-40 (*B*) Tg+ and Tg− mice fed either an HFD or ND from 6 to 16 weeks of age. Six to 10 mice per group were tested for glucose tolerance at 16 weeks (1.5 mg glucose/g body weight), and blood glucose was measured at the indicated times after injection. *Significant difference from Tg− animals on the same diet at $P < 0.05$.

is supported by the recently described importance of ZNT3 for insulin secretion (28) and ZNT5 in models of T1DM (3).

ZnT8 null mice (global or β-cell) have a substantial reduction in Zn^{2+}, but little effect on glucose tolerance and no effect on insulin (10,27). However, in β-cell *ZnT8* knockouts, proinsulin levels are increased, whereas proinsulin transcription, and its transcription factors (pdx1, mafA) and processing enzyme RNAs (proconvertases 1/3 and 2 carboxypeptidase E), are decreased (27). We suspect that, as with T1DM, too little or too much Zn^{2+} is detrimental for T2DM, with a partial Zn^{2+} reduction being optimal (3). *ZnT8* global or β-cell knockouts reduce Zn^{2+} most, followed by *ZnT8 RW* overexpression (dominant negative) and *ZnT8* knockdown, which have modestly reduced Zn^{2+} levels, versus *ZnT8 WT* overexpression, which has high Zn^{2+} levels. Varying the pancreatic ZnT8WT/Zn^{2+} levels affect insulin staining and may be mediated in part by effects of Zn^{2+} to inhibit processing of proinsulin to insulin as demonstrated by proinsulin and insulin immunohistochemistry.

Elevated proinsulin levels are associated with increased risk of T2DM in humans (8), and homozygous carriers of the *ZnT8 WT* risk allele had elevated proinsulin/insulin ratios in humans (7). Overexpression of *ZnT8 WT* in Tg mice results in an increase in Zn^{2+} and proinsulin staining and a decrease in insulin staining and glucose tolerance. hZNT8RW significantly reduces pancreatic Zn^{2+} and proinsulin levels and increases insulin and glucose tolerance (Figs. 3 and 4 and Table 2), which differentiates this mechanism from others that effect insulin sensitivity. We hypothesize that hZNT8RW forms hypoactive heterodimers with mZNT8, or perhaps with mZNT5, mZNT6, or mZNT7, which are all expressed in the endoplasmic reticulum and Golgi. Generally, an HFD demonstrated more substantial variations in Zn^{2+}, insulin, or proinsulin

enhances basal glucose–stimulated insulin secretion (26). Thus, ZNT8 functions to sequester Zn^{2+} into the secretory granules of β-cells analogous to ZNT3 in presynaptic secretory granules in the brain. ZNT8 may also function in heterodimers with ZNT5, -6, and -7 to put Zn^{2+} into the secretory granules of β-cells during their formation in the Golgi.

A common single nucleotide polymorphism in *ZnT8*, which changes R325 to W, is associated with a reduced risk for T2DM (5,6). This nonconservative substitution of a charged basic amino acid for a hydrophobic polar amino acid occurs at the predicted transporter dimer interface in an important modulatory region (10). The R325W protein causes reduced Zn^{2+} staining when overexpressed in β-cells, suggesting that it acts as a dominant negative, dimerizing with itself or other ZnTs and reducing their transport function. A knockout of *ZnT8* demonstrates a small reduction in glucose tolerance and a change in secretory granule morphology (10,27). These results suggest a functional redundancy in secretory Zn^{2+} transporters, and this redundancy
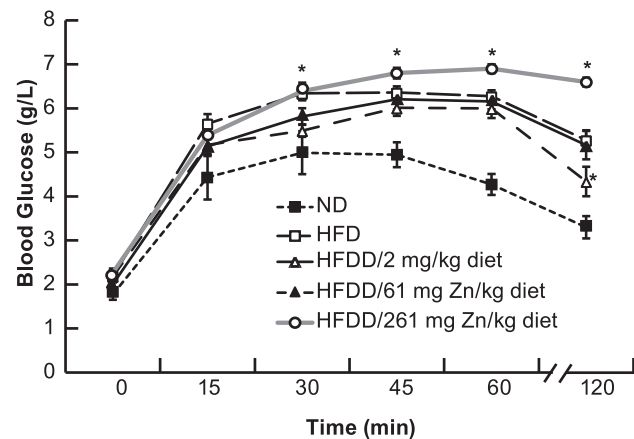

Figure 4—Intraperitoneal glucose tolerance in C57BL/6J mice fed an HFD, ND, or HFDD/2, HFDD/61, or HFDD/261 mg Zn^{2+}/kg diet from 6 to 16 weeks of age. Six to 10 mice per group were tested for glucose tolerance at 16 weeks (1.5 mg glucose/g body weight), and blood glucose was measured at the indicated times after injection. *Significant difference from HFDD/61 mg Zn^{2+}/kg diet at $P < 0.05$.
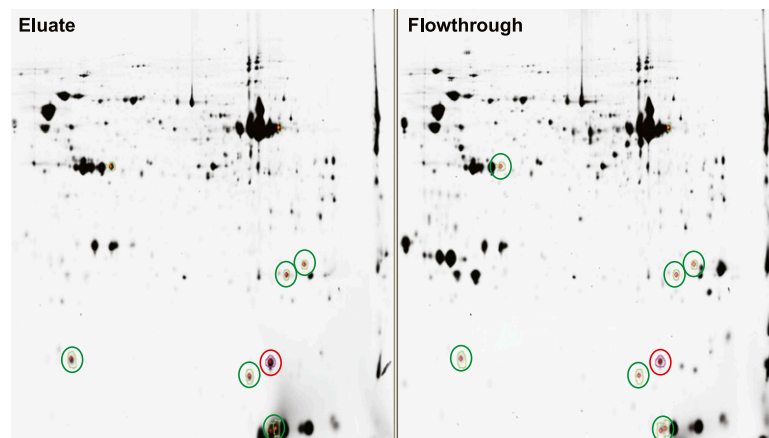
Figure 5—Two-dimensional gels of ZBPs from control pancreas. Fifty micrograms of the input, flowthrough, and eluate from Zn^{2+}-agarose columns of pancreatic extracts from control animals was precipitated; labeled with Cy5, Cy3, and Cy2, respectively; and loaded onto protein isoelectric focusing tube gels before running on SDS-PAGE gels in the second dimension. The left panel shows the Cy2-labeled eluate proteins. The right panel shows the Cy3-labeled proteins from the flowthrough fraction. Protein spots fivefold enriched in eluate and containing sufficient mass were picked (faint colored circles) and identified using liquid chromatography–mass spectrometry (Table 1).

stainings compared with a ND, suggesting an interaction between zinc levels and the effects of high fat. Reducing Zn^{2+} in the diet is less effective than the RW Tg mouse models to increase glucose tolerance. However, increasing Zn^{2+} in the diet is at least as effective as the hZNT8WT Tg mouse model to decrease glucose tolerance after HFD (Fig. 4).

Our data show that the levels of proinsulin and insulin are inversely modulated by Zn^{2+}, suggesting the conversion of proinsulin to insulin is inhibited by Zn^{2+}. The processing enzymes that convert proinsulin to insulin (proconvertases 1/3 and 2 and carboxypeptidase E) have been shown to be Ca^{2+} dependent (29), and therefore Zn^{2+} levels could affect proinsulin processing by competition with Ca^{2+}. Alternatively, proinsulin transcription could be Zn^{2+} modulated, but this should cause covariance of proinsulin and insulin. Proinsulin processing enzyme transcription could be Zn^{2+} modulated, and cytoplasmic/nuclear Zn^{2+} activates various kinase cascades impinging on transcription (30–32). Also the insulin-degrading enzyme proteinase III requires Zn^{2+} for activity (33), and membrane-associated insulin-degrading activity is activated by Zn^{2+} (34). We postulate that ZNT8RW mediates a moderate reduction in pancreatic Golgi Zn^{2+} levels, reducing competition for required Ca^{2+} binding sites on proinsulin processing enzymes and inducing less Zn^{2+}-dependent insulin degradation, thereby decreasing proinsulin levels and increasing insulin levels and glucose tolerance.

To understand this process, we identified pancreatic ZBPs. The role of α-amylase as a ZBP is interesting because it is a major pancreatic protein that requires Zn^{2+} for activity, may be secreted in the apo form from α-cells, and loads with Zn^{2+} that is released from β-cells (35). This would provide a cross talk/signaling mechanism between α- and β-cells and suggests a mechanism for excessive Zn^{2+}

excretion in T1DM and T2DM (36). Isolating α-amylase and CpA1 provides confidence that the technique is working, and inclusion of excess zinc prevented purification of these ZBPs (data not shown). Several of the ZBPs identified were energy metabolic enzymes and/or mitochondrial proteins, confirming a role of energy metabolism in diabetes. Glutathione S-transferase-μ is one of the ZBPs identified in the control pancreas. Another ZBP identified was MMSDH, which is mitochondrial in origin and displays diabetes- and enalapril-sensitive tyrosine nitration (37). By catalyzing the CoA- and $NADP^+$-dependent oxidative

Table 2—Identification of the control pancreatic ZBPs

Protein	Score[1]	n of peptide matches	MW (kD)[2]
α-Amylase	656	29	58.1
NDPKA	431	21	17.3
NDPKB	419	25	17.5
MMSDH	328	8	58.3
CpA1	182	6	47.5
Glutathione S-transferase-μ 1	175	7	26.1
Eukaryotic translation initiation factor 5A-1	126	7	17.0
α-Aminoadipic semialdehyde dehydrogenase	96	1	59.3
SCOT	87	3	56.4

[1]A score >70 gives >95% confidence that the protein was present in the picked protein spot from the two-dimensional gel. The score was based upon the number of peptides identified for the given protein and the intensity of that peptide. [2]Calculated size in kD from the protein sequence was given as molecular weight (MW).
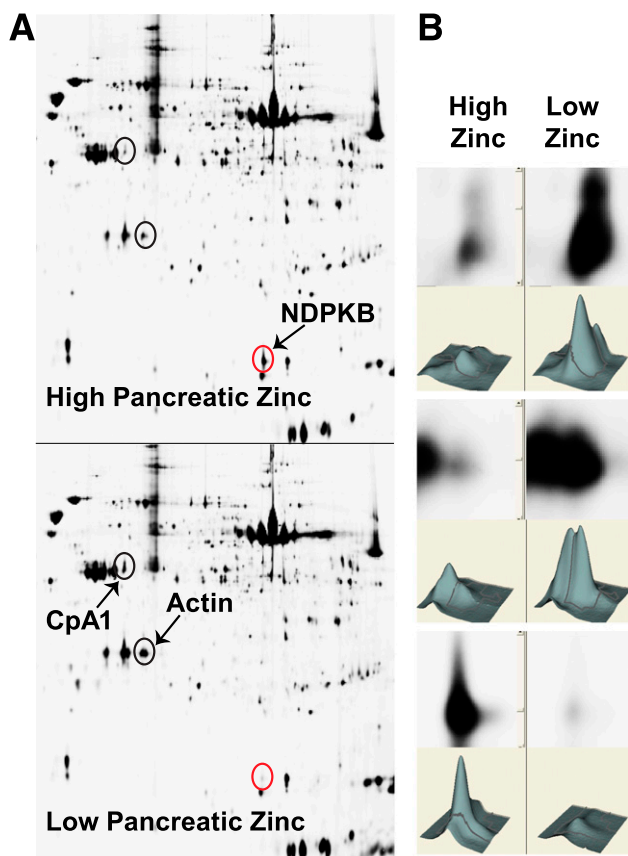
Figure 6—Two-dimensional protein isoelectric focusing/SDS-PAGE gels of the zinc-agarose eluates of high-zinc (hZnT8WT) pancreas vs. low-zinc (hZnT8RW) pancreas. Fifty micrograms of the high-zinc E1, high-zinc FT, and low-zinc E1 fractions were processed. Protein spots fivefold enriched in an eluate and containing sufficient mass were picked and identified using liquid chromatography–mass spectrometry. Blue circles were increased in low zinc, and the red circles were increased in high-zinc conditions. The right panel shows the three circled spots at high magnification, with histograms.

decarboxylation of malonate semialdehyde to acetyl-CoA, MMSDH provides a nonglycolytic means for producing acetyl-CoA. α-Aminoadipic semialdehyde dehydrogenase is involved in the metabolism of lysine. SCOT is a mitochondrial enzyme that catalyzes the reversible transfer of CoA from acetoacetyl-CoA to succinate to form acetoacetate and succinyl-CoA, a reaction in the gluconeogenesis pathway. Physiologically, its enzymatic activity is involved in maintaining the blood glucose level (38).

CpA1 is a soluble zinc-dependent enzyme synthesized in the pancreas and secreted into the gastrointestinal tract where its activity is modulated by dietary zinc (39). CpA1 is a known Zn^{2+} metallopeptidase and belongs to a family of enzymes that process proinsulin. CpA1 is differentially increased in low pancreatic Zn^{2+} (ZnT8RW), supporting our hypothesis that reduced pancreatic Zn^{2+} in the HFD model of T2DM could be beneficial by inducing proinsulin maturation by CpA1 processing of enzymes involved.

NDPKB is critically involved in the diabetic process by modulating its isoenzyme activities and those of AMPK. NDPKA has been shown to be phosphorylated and inactivated by AMPK and to also modulate AMPK function (40). AMPK is the major checkpoint for energy metabolism inducing ATP synthetic proteins and reducing pathways that consume ATP and is critically involved in the diabetic process (reviewed in Rutter and Leclerc [41]). NDPKB is differentially increased in high pancreatic zinc conditions (Fig. 6). NDPKB also has many functions related to cellular proliferation of immune cells (42–44).

These results show that pancreatic Zn^{2+} and proinsulin levels covary but are inversely variant with insulin and glucose tolerance in the HFD model of T2DM. We identified pancreatic ZBPs and determined those differentially affected by zinc concentrations as therapeutic targets. We also suggest that ZNT8RW acts in a dominant-negative manner to reduce pancreatic Zn^{2+} levels and that proinsulin and insulin processing are likely involved in the beneficial effects of this polymorphism, which we will test in future studies.

References

1. Kim BJ, Kim YH, Kim S, et al. Zinc as a paracrine effector in pancreatic islet cell death. Diabetes 2000;49:367–372

2. Priel T, Aricha-Tamir B, Sekler I. Clioquinol attenuates zinc-dependent beta-cell death and the onset of insulitis and hyperglycemia associated with experimental type I diabetes in mice. Eur J Pharmacol 2007;565:232–239

3. Sheline CT, Shi C, Takata T, et al. Dietary zinc reduction, pyruvate supplementation, or zinc transporter 5 knockout attenuates β-cell death in nonobese diabetic mice, islets, and insulinoma cells. J Nutr 2012;142:2119–2127

4. Taylor CG. Zinc, the pancreas, and diabetes: insights from rodent studies and future directions. Biometals 2005;18:305–312

5. Sladek R, Rocheleau G, Rung J, et al. A genome-wide association study identifies novel risk loci for type 2 diabetes. Nature 2007;445:881–885

6. Scott LJ, Mohlke KL, Bonnycastle LL, et al. A genome-wide association study of type 2 diabetes in Finns detects multiple susceptibility variants. Science 2007;316:1341–1345

7. Majithia AR, Jablonski KA, McAteer JB, et al.; DPP Research Group. Association of the SLC30A8 missense polymorphism R325W with proinsulin levels at baseline and after lifestyle, metformin or troglitazone intervention in the Diabetes Prevention Program. Diabetologia 2011;54:2570–2574

8. Wareham NJ, Byrne CD, Williams R, Day NE, Hales CN. Fasting proinsulin concentrations predict the development of type 2 diabetes. Diabetes Care 1999; 22:262–270

9. Wenzlau JM, Moua O, Liu Y, Eisenbarth GS, Hutton JC, Davidson HW. Identification of a major humoral epitope in Slc30a8 (ZnT8). Ann N Y Acad Sci 2008;1150:252–255

10. Nicolson TJ, Bellomo EA, Wijesekara N, et al. Insulin storage and glucose homeostasis in mice null for the granule zinc transporter ZnT8 and studies of the type 2 diabetes-associated variants. Diabetes 2009;58:2070–2083

11. Huang XF, Arvan P. Intracellular transport of proinsulin in pancreatic beta-cells. Structural maturation probed by disulfide accessibility. J Biol Chem 1995; 270:20417–20423

12. Chung J, Nguyen AK, Henstridge DC, et al. HSP72 protects against obesity-induced insulin resistance. Proc Natl Acad Sci U S A 2008;105:1739–1744

13. Miyazaki J, Araki K, Yamato E, et al. Establishment of a pancreatic beta cell line that retains glucose-inducible insulin secretion: special reference to expression of glucose transporter isoforms. Endocrinology 1990;127:126–132

14. Moynihan KA, Grimm AA, Plueger MM, et al. Increased dosage of mammalian Sir2 in pancreatic beta cells enhances glucose-stimulated insulin secretion in mice. Cell Metab 2005;2:105–117

15. Chimienti F, Devergnas S, Favier A, Seve M. Identification and cloning of a beta-cell-specific zinc transporter, ZnT-8, localized into insulin secretory granules. Diabetes 2004;53:2330–2337

16. Han JH, Stratowa C, Rutter WJ. Isolation of full-length putative rat lysophospholipase cDNA using improved methods for mRNA isolation and cDNA cloning. Biochemistry 1987;26:1617–1625

17. Alban A, David SO, Bjorkesten L, et al. A novel experimental design for comparative two-dimensional gel analysis: two-dimensional difference gel electrophoresis incorporating a pooled internal standard. Proteomics 2003;3: 36–44

18. Kojima H, Fujimiya M, Terashima T, Kimura H, Chan L. Extrapancreatic proinsulin/insulin-expressing cells in diabetes mellitus: is history repeating itself? Endocr J 2006;53:715–722

19. Taylor KM, Nicholson RI. The LZT proteins; the LIV-1 subfamily of zinc transporters. Biochim Biophys Acta 2003;1611:16–30

20. Palmiter RD, Huang L. Efflux and compartmentalization of zinc by members of the SLC30 family of solute carriers. Pflugers Arch 2004;447:744–751

21. Suzuki T, Ishihara K, Migaki H, et al. Two different zinc transport complexes of cation diffusion facilitator proteins localized in the secretory pathway operate to activate alkaline phosphatases in vertebrate cells. J Biol Chem 2005;280:30956–30962

22. Bai S, Sheline CR, Zhou Y, Sheline CT. A reduced zinc diet or zinc transporter 3 knockout attenuate light induced zinc accumulation and retinal degeneration. Exp Eye Res 2013;108:59–67

23. Suh SW, Hamby AM, Gum ET, et al. Sequential release of nitric oxide, zinc, and superoxide in hypoglycemic neuronal death. J Cereb Blood Flow Metab 2008;28:1697–1706

24. Huang L, Gitschier J. A novel gene involved in zinc transport is deficient in the lethal milk mouse. Nat Genet 1997;17:292–297

25. Inoue K, Matsuda K, Itoh M, et al. Osteopenia and male-specific sudden cardiac death in mice lacking a zinc transporter gene, Znt5. Hum Mol Genet 2002;11:1775–1784

26. Chimienti F, Devergnas S, Pattou F, et al. In vivo expression and functional characterization of the zinc transporter ZnT8 in glucose-induced insulin secretion. J Cell Sci 2006;119:4199–4206

27. Wijesekara N, Dai FF, Hardy AB, et al. Beta cell-specific Znt8 deletion in mice causes marked defects in insulin processing, crystallisation and secretion. Diabetologia 2010;53:1656–1668

28. Smidt K, Jessen N, Petersen AB, et al. SLC30A3 responds to glucose- and zinc variations in beta-cells and is critical for insulin production and in vivo glucose-metabolism during beta-cell stress. PLoS One 2009;4:e5684

29. Davidson HW, Rhodes CJ, Hutton JC. Intraorganellar calcium and pH control proinsulin cleavage in the pancreatic beta cell via two distinct site-specific endopeptidases. Nature 1988;333:93–96

30. Park JA, Koh JY. Induction of an immediate early gene egr-1 by zinc through extracellular signal-regulated kinase activation in cortical culture: its role in zinc-induced neuronal death. J Neurochem 1999;73:450–456

31. Kim S, Jung Y, Kim D, Koh H, Chung J. Extracellular zinc activates p70 S6 kinase through the phosphatidylinositol 3-kinase signaling pathway. J Biol Chem 2000;275:25979–25984

32. Manzerra P, Behrens MM, Canzoniero LM, et al. Zinc induces a Src family kinase-mediated up-regulation of NMDA receptor activity and excitotoxicity. Proc Natl Acad Sci U S A 2001;98:11055–11061

33. Becker AB, Roth RA. Identification of glutamate-169 as the third zinc-binding residue in proteinase III, a member of the family of insulin-degrading enzymes. Biochem J 1993;292:137–142

34. Bellomo G, Nicotera PL, Travaglino F, Palma Martino A, Mirabelli F, Fratino P. Insulin degradation in human erythrocyte: effects of cations. Acta Diabetol Lat 1985;22:63–69

35. Lü J, Combs GF Jr. Effect of excess dietary zinc on pancreatic exocrine function in the chick. J Nutr 1988;118:681–689

36. Chausmer AB. Zinc, insulin and diabetes. J Am Coll Nutr 1998;17:109–115

37. Ishii N, Carmines PK, Yokoba M, et al. Angiotensin-converting enzyme inhibition curbs tyrosine nitration of mitochondrial proteins in the renal cortex during the early stage of diabetes mellitus in rats. Clin Sci (Lond) 2013;124:543–552

38. Berry GT, Fukao T, Mitchell GA, et al. Neonatal hypoglycaemia in severe succinyl-CoA: 3-oxoacid CoA-transferase deficiency. J Inherit Metab Dis 2001; 24:587–595

39. Fernández D, Boix E, Pallarès I, Avilés FX, Vendrell J. Structural and functional analysis of the complex between citrate and the zinc peptidase carboxypeptidase A. Enzyme Res 2011;2011:128676

40. Muimo R, Crawford RM, Mehta A. Nucleoside diphosphate kinase A as a controller of AMP-kinase in airway epithelia. J Bioenerg Biomembr 2006;38: 181–187

41. Rutter GA, Leclerc I. The AMP-regulated kinase family: enigmatic targets for diabetes therapy. Mol Cell Endocrinol 2009;297:41–49

42. Di L, Srivastava S, Zhdanova O, Sun Y, Li Z, Skolnik EY. Nucleoside diphosphate kinase B knock-out mice have impaired activation of the K+ channel KCa3.1, resulting in defective T cell activation. J Biol Chem 2010;285:38765–38771

43. Srivastava S, Zhdanova O, Di L, et al. Protein histidine phosphatase 1 negatively regulates CD4 T cells by inhibiting the K+ channel KCa3.1. Proc Natl Acad Sci U S A 2008;105:14442–14446

44. Postel EH, Wohlman I, Zou X, et al. Targeted deletion of Nm23/nucleoside diphosphate kinase A and B reveals their requirement for definitive erythropoiesis in the mouse embryo. Dev Dyn 2009;238:775–787